A Lagrangian model for turbulent dispersion with turbulent-like flow structure: Comparison with direct numerical simulation for two-particle statistics

Nadeem A. Malik[a] and J. C. Vassilicos[b]
Department of Applied Mathematics and Theoretical Physics, University of Cambridge, Cambridge CB3 9EW, England

(Received 3 April 1998; accepted 26 February 1999)

A wide range of relative two-particle dispersion statistics from the Lagrangian Kinematic Simulation (KS) model, which contains turbulent-like flow structures, compares well with Yeung's [Phys. Fluids **6**, 3416 (1994)] DNS results. In particular, the Lagrangian flatness factor $\mu_4(t)$ compares excellently (better than Heppe's [J. Fluid Mech. **357**, 167 (1998)] nonlinear stochastic model). For higher Reynolds numbers the results from KS show that $\mu_4(t)$ is significantly greater than 3 over a wide range of times within the inertial range of time scales. © *1999 American Institute of Physics.* [S1070-6631(99)02706-3]

I. INTRODUCTION

We compare the results of a Kinematic Simulation (KS) with Yeung's[1] Direct Numerical Simulation (DNS) results on two-particle dispersion. KS is a *Lagrangian* model of turbulent dispersion that incorporates turbulent-like flow structure (see Fung *et al.*,[2] Fung and Vassilicos,[3] and references therein). The basic assumption of KS is that it should be sufficient, for the calculation of Lagrangian (*not* Eulerian) statistics, to have a qualitatively (but not necessarily quantitatively) realistic representation of the geometrical character of turbulent trajectories that are generated by the flow structures of the turbulence. The flow structures in KS are not quantitatively precise, but they are turbulent-like in the sense that they are the type of eddying, straining, and streaming structures similar to those expected and observed in turbulent flows; see Chong *et al.*,[4] for example. The KS structures are not quantitatively precise, in the sense that they do not have exactly the same shape as the equivalent structures in the real turbulence.

Yeung's[1] results on two-particle relative dispersion have been obtained from a DNS of a statistically stationary and isotropic turbulence with $\mathrm{Re}_\lambda \approx 91$. These results include relative displacements, correlation coefficients, skewness coefficients, and flatness factors. Of particular interest is the result on the time dependence of the flatness factor $\mu_4(t,l_0)=\langle w_1^4(t)\rangle/\langle w_1^2(t)\rangle^2$, where w_1 is one arbitrary component of the relative velocity $\mathbf{w}(t)=\mathbf{u}^{(1)}(t)-\mathbf{u}^{(2)}(t)$ between two fluid elements (particles) marked (1) and (2) with respective Lagrangian velocities $\mathbf{u}^{(1)}(t)$ and $\mathbf{u}^{(2)}(t)$, l_0 is the initial separation of the two particles, and the brackets $\langle\cdots\rangle$ denote an average over an ensemble of fluid element pairs. The one stochastic model of two-particle dispersion to date that has been adjusted to incorporate finite Reynolds number effects (Heppe[5]) gives, for $\mathrm{Re}_\lambda \approx 91$, a time dependence of μ_4 that is qualitatively similar to Yeung's,[1] but that differs quantitatively by nearly one order of magnitude. KS is, by construction, a finite Reynolds number model, and we report here that KS can reproduce the results of Yeung's[1] DNS within good quantitative agreement, including the result on $\mu_4(t)$.

In Sec. II we describe KS and briefly contrast it to stochastic models of turbulent dispersion. In Sec. III we present the results obtained with KS and we compare them to the DNS results obtained by Yeung[1] for $\mathrm{Re}_\lambda \approx 91$. In Sec. IV we use KS to calculate $\mu_4(t)$ for several higher Reynolds numbers. This leads us to a short discussion of Lagrangian Intermittency, and we conclude in Sec. V.

II. KINEMATIC SIMULATIONS

KS is a Lagrangian model of turbulent dispersion, where individual fluid element trajectories $\mathbf{x}(t)$ are calculated by integrating

$$\frac{d}{dt}\mathbf{x}(t)=\mathbf{u}(t)=\mathbf{u}_\mathrm{E}[\mathbf{x}(t),t], \tag{1}$$

in individual realizations of an Eulerian turbulent-like velocity field $\mathbf{u}_\mathrm{E}(\mathbf{x},t)$, which is three dimensional for the purposes of this paper, and is generated as follows:

$$\mathbf{u}_\mathrm{E}(\mathbf{x},t)=\sum_{n=1}^{N_k}[\mathbf{A}_n\times\hat{\mathbf{k}}_n\cos(\mathbf{k}_n\cdot\mathbf{x}+\omega_n t) + \mathbf{B}_n\times\hat{\mathbf{k}}_n\sin(\mathbf{k}_n\cdot\mathbf{x}+\omega_n t)], \tag{2}$$

where N_k is the number of modes in the simulation, $\hat{\mathbf{k}}_n$ is a random unit vector ($\mathbf{k}_n=k_n\hat{\mathbf{k}}_n$), and the directions and orientations of $\mathbf{A}_n$ and $\mathbf{B}_n$ are chosen randomly under the constraint that they be normal to $\hat{\mathbf{k}}_n$. This random choice of directions for the nth wave mode is independent of the ran-

[a]Electronic mail: N. A. Malik@damtp.cam.ac.uk. Also at the Department of Mathematics, Hong Kong University of Science & Technology, Clear Water Bay, Kowloon, Hong Kong.
[b]Electronic mail: J.C.Vassilicos@damtp.cam.ac.uk

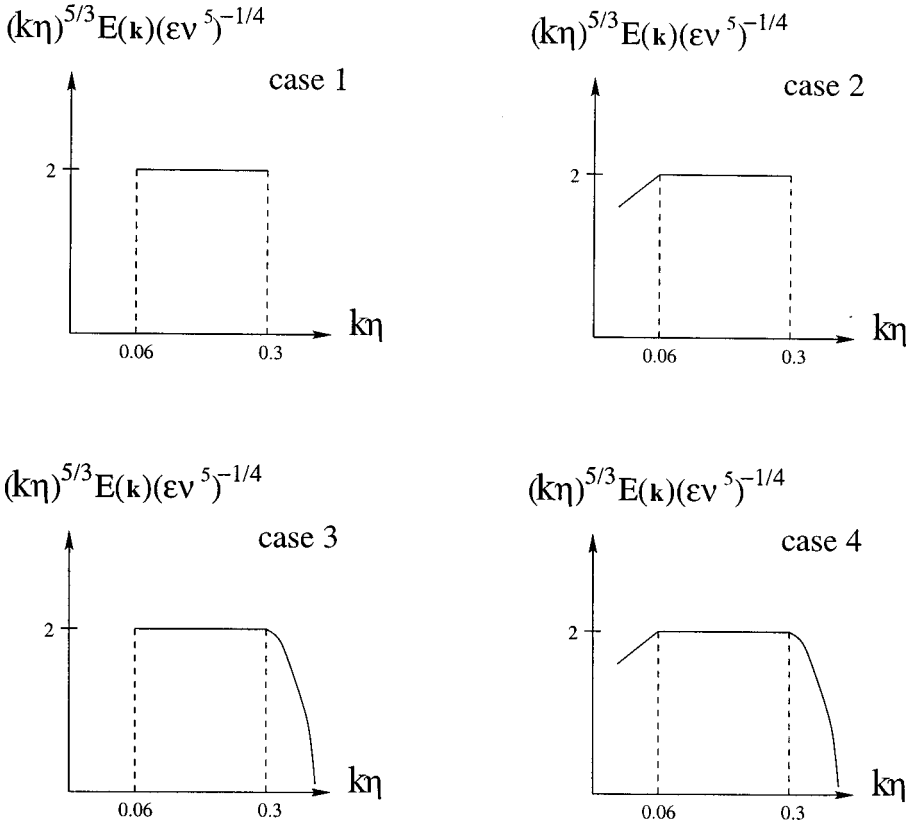

FIG. 1. The different KS energy spectra used in the simulations. Details of each case 1–4 is described in the first paragraph of Sec. III.

dom choice of directions for all other wave modes. Note that the velocity field (2) is incompressible by construction. The positive amplitudes A_n and B_n of the vectors $\mathbf{A}_n$ and $\mathbf{B}_n$ are determined by

$$\tfrac{3}{2}A_n^2=\tfrac{3}{2}B_n^2=E(k_n)\Delta k_n, \tag{3}$$

where $E(k)$ is an arbitrarily prescribed Eulerian energy spectrum, and $\Delta k_n=(k_{n+1}-k_{n-1})/2$ for $2\leqslant n\leqslant N_k-1$, $\Delta k_1=(k_2-k_1)/2$, and $\Delta k_{N_k}=(k_{N_k}-k_{N_{k-1}})/2$. Within a simulated inertial subrange, we choose $(k\eta)^{5/3}E(k)(\epsilon\nu^5)^{-1/4}=\alpha_{\mathrm{K}}$, where α_{K} is a dimensionless constant and ϵ is a quantity that has the dimensions of a rate of energy dissipation (although in KS there is no actual dynamical transfer of energy between modes) and is given formally by $2\nu\int_0^\infty k^2E(k)dk$. We can also obtain $(u')^2/v_\eta^2=2\int_0^\infty E(k)dk$, where $v_\eta=(\epsilon\eta)^{1/3}$. From the energy spectrum in Fig. 1 of Yeung,[1] we have $\alpha_{\mathrm{K}}=2$. As in Yeung,[1] all quantities are scaled on the Kolmogorov microscales of length and time, η and $\tau_\eta=\epsilon^{-1/3}\eta^{2/3}$, unless otherwise stated. Note that Yeung defines η from $\eta k_\eta=1.5$, and we do the same; see Fig. 1. More details are contained in Table I.

The frequencies ω_n in (2) determine the unsteadiness associated with wave mode n. In this particular version of KS, we choose the unsteadiness frequency ω_n to be proportional to the eddy-turnover time of the wave mode n, i.e.,

$$\omega_n=\lambda\sqrt{k_n^3E(k_n)}, \tag{4}$$

where λ is a dimensionless constant that may be expected to be of order 1. (If $\lambda\gg1$ then the velocity field is essentially flapping so fast at all scales that fluid elements do not have the time to experience the effects of eddying, streaming, and straining flow structures, and if $\lambda\ll1$ then the velocity field is essentially frozen at all scales, which is unlike turbulence.)

The inputs of KS are therefore the Eulerian energy spectrum $E(k)$, the unsteadiness parameter λ, and, strictly speaking, also the number of modes N_k and the distribution of wave numbers k_n. For example, in this work we use geometric distributions, i.e., $k_n=k_1a^{n-1}$, where a is a dimensionless number determined by $k_{N_k}=k_1a^{N_{k-1}}$, because extreme wave numbers k_1 and k_{N_k} are given with the energy spectrum $E(k)$. However, there is no absolute freedom to chose these input parameters as we wish: λ cannot be larger than $O(1)$, and changes in the distribution and number N_k of modes should not significantly affect the Lagrangian outputs of the model.

Previous works (Fung *et al.*,[2] Fung and Vassilicos,[3] and references therein) have shown that turbulent-like velocity fields of the type simulated here are statistically stationary in time, and also isotropic. These works have also shown that instantaneous streamlines defined by the KS velocity field (2) have well-defined eddying, straining, and streaming flow structures and suggested that the mere existence of these flow structures has important quantitative implications on

TABLE I. Input KS parameter values for case 4 of Fig. 1.

Case	k_I/k_{L}	$k_0\eta$	$N_{k\mathrm{L}}$	$k_{\mathrm{L}}\eta$	N_{kI}	$k_I\eta$	N_{kH}	$k_\eta\eta$
4	5	1.72×10^{-2}	50	6.0×10^{-2}	50	0.3	5	1.5
4	100	8.57×10^{-4}	50	3.0×10^{-3}	150	0.3	5	1.5
4	400	2.14×10^{-4}	50	7.5×10^{-4}	250	0.3	5	1.5

Lagrangian two-particle statistics. At any rate, the mechanisms by which particles separate under the action of a stochastic Lagrangian relative velocity process or under the action of a Eulerian velocity field with well-defined small-scale turbulent-like flow structures, as in KS, are very different. We briefly describe stochastic models of turbulent dispersion before spelling out this difference.

Stochastic models of turbulent dispersion are Lagrangian models where particle positions in the case of one-particle models, and two-particle relative velocities in the case of two-particle models, are solutions of Langevin equations and thereby depend on Wiener processes (see Heppe,[5] Pedrizzetti and Novikov,[6] Borgas and Sawford,[7] and references therein). Such Lagrangian positions and relative velocities vary with time in a way similar to a Brownian motion with drift, and are therefore very different in character from the Lagrangian positions and velocities generated by the KS velocity field (2). Even though statistics are obtained by averaging over many particle trajectories in many realizations of the turbulence, the qualitative difference in the nature of the Lagrangian velocity processes and consequently in the nature of particle trajectories, can have a significant quantitative impact on some of these statistics (see Fung *et al.*,[2] Malik,[8] and Fung and Vassilicos[3]). This is quite dramatically demonstrated in this paper, where we show that KS can reproduce Yeung's[1] DNS flatness factor $\mu_4(t)$ results within a factor of about 1.5, whereas Heppe's[2] two-particle stochastic model of dispersion gets it to within a factor of about 8. As discussed by Fung *et al.*[2] and Fung and Vassilicos,[3] in KS, particle pairs move alongside each other for quite some time until they encounter a straining region and suddenly separate. Experimental measurements of one- and two-particle pair trajectories in turbulent flows has been obtained recently by Virant and Dracos[9] using the three-dimensional (3-D) Particle Tracking Velocimetry technique developed at the ETH Zürich, (Maas *et al.*[10] and Malik *et al.*[11]). Most relevant to the present work is their Fig. 8(d), which shows the trajectories of a pair of particles initially close together: they remain close together for some time before bursting away from each other in a similar manner to that just described. The separation of particle pairs in stochastic models does not happen in bursts, but more uniformly in time because of the Wiener processes' Markovian property.

Another important difference between KS and stochastic models of turbulent dispersion is that the Lagrangian integral time scale T_L is an input for stochastic models, but it is an output in KS. Furthermore, KS is a Lagrangian model of turbulent dispersion that can be used unaltered both for one-particle and two-particle dispersion, whereas stochastic models of one-particle and two-particle dispersion need to be constructed separately.

III. RESULTS AND COMPARISON WITH DNS

Yeung's DNS is for statistically stationary turbulence, and the energy spectrum remains, therefore, constant in time. This energy spectrum—Fig. 1 in Yeung[1]—is approximately equal to $2(\epsilon\nu^5)^{1/4}(k\eta)^{-5/3}$ in the range $0.06 \leqslant k\eta \leqslant 0.3$, where η is the Kolmogorov length scale, ϵ the energy dissipation rate per unit mass, and ν the kinematic viscosity. But there is also some energy in the low ($k\eta < 0.06$) and in the high ($k\eta > 0.3$) wave number ranges of the spectrum. Hence, we have experimented with four different spectral inputs for KS. Common to all these inputs is that $E(k) = 2(\epsilon\nu^5)^{1/4}(k\eta)^{-5/3}$ in the range $0.06 \leqslant k\eta \leqslant 0.3$ with a number of modes $N_{kI} = 50$ (where the subscript I stands for Inertial). In case 1, $E(k) = 0$ for all other wave numbers; in case 2, $E(k) = 0$ for $k\eta > 0.3$ but is nonzero and equal to Yeung's low-wave number spectrum for $k\eta < 0.06$ with a number of modes $N_{kL} = 50$ (where the subscript L stands for low-wave number); in case 3, $E(k) = 0$ for $k\eta < 0.06$ but is nonzero and equal to Yeung's high-wave number spectrum for $k\eta > 0.3$ with a number of modes $N_{kH} = 5$ (where the subscript H stands for high-wave number); and in case 4, $E(k)$ is equal to Yeung's energy spectrum over the entire wave number range, with $N_{kL} = 50$ modes, where $k\eta < 0.06$, $N_{kI} = 50$ modes, where $0.06 \leqslant k\eta \leqslant 0.3$ and $N_{kH} = 5$ modes, where $k\eta > 0.3$. These energy spectra are summarized in Fig. 1, and Table I gives additional details of the KS input parameters. In terms of wave modes, the three distinct spectral ranges are the following: (1) the low-wave number range $k_0 \leqslant k \leqslant k_L$ ($k_L/k_0 = 3.5$, $k_L\eta = 0.06$); (2) the inertial range $k_L \leqslant k \leqslant k_I$ ($k_I/k_L = 5$, $k_I\eta = 0.3$); (3) the high-wave number range $k_I \leqslant k \leqslant k_\eta$ ($k_\eta/k_I = 5$, $k_\eta\eta = 1.5$). The number of modes in the input cases 1 to 4 varies between $N_{kI} = 50$ (case 1) and $N_{kL} + N_{kI} + N_{kH} = 105$ (case 4). Compared to the number of excited wave number modes in Yeung's DNS, which is $128^3 \approx 2 \times 10^6$, this is a staggering reduction by a factor of four orders of magnitude, particularly because the results reported here show good agreement in the Lagrangian statistics between KS and DNS.

We have verified that there is no significant variability in most of our results when the unsteadiness parameter λ is progressively changed from 0 to 1, and the specific results presented in this paper are those that have been obtained for $\lambda = 0.4$. For many of the statistics presented below, even a *steady* KS model (i.e., $\lambda = 0$) compares favorably with Yeung's DNS [see Malik,[8,12] who first observed that the two-particle dispersion $\langle|\Delta\mathbf{l}|^2\rangle$ (defined in the next paragraph) is insensitive to the unsteadiness in the range $0 \leqslant \lambda \leqslant 1$ in 3-D KS].

We now describe these results. The separation vector between fluid elements (1) and (2) at respective locations $\mathbf{x^{(1)}(t)}$ and $\mathbf{x^{(2)}(t)}$ at time t is $\mathbf{l(t)} = \mathbf{x^{(1)}(t)} - \mathbf{x^{(2)}(t)}$, [$l_0 = |\mathbf{l}(0)|$], and the relative displacement is $\Delta\mathbf{l}(t) = \mathbf{l}(t) - \mathbf{l}(0)$. In Fig. 2, we compare Yeung's DNS and the KS (case 4, Fig. 1) results for $\langle|\Delta\mathbf{l}|^2\rangle^{1/2}/\eta$ against t/τ_η for the same six initial separations, $l_0/\eta = \frac{1}{4}$,1,4,16,32,64, where τ_η is the Kolmogorov time scale, and the brackets $\langle\cdots\rangle$ denote an average over many fluid element pairs in many different realizations of the KS Eulerian velocity field $\mathbf{u}_E(\mathbf{x},t)$. In all of our comparisons with Yeung's Lagrangian statistics, we compute the same number of particle pair trajectories, 18 432, to make our ensemble effectively identical to Yeung's. However, whereas Yeung computes the entire ensemble of particle pair trajectories drawn from a *single realization of a DNS flow field*, we compute *one* set of particle pair trajectories *per KS flow field realization*, so that our

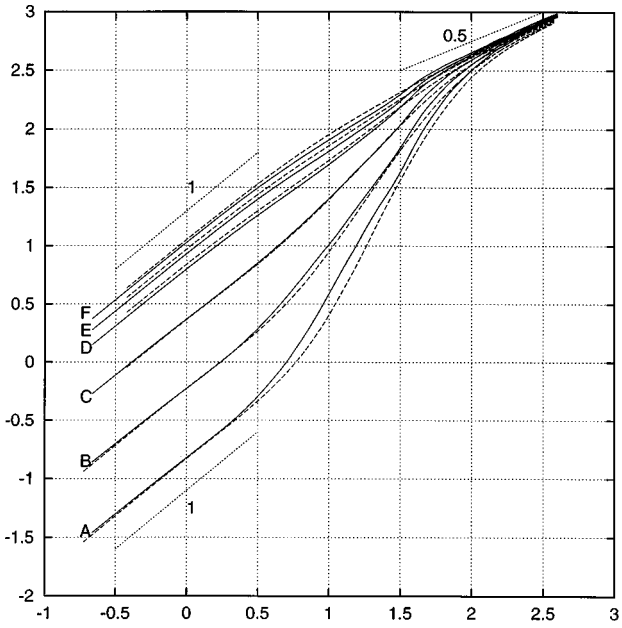

FIG. 2. Growth of the rms relative separation, $\langle \Delta l_i \, \Delta l_i \rangle^{1/2}/\eta$, versus the diffusion time t/τ_η. η and τ_η are the Kolmogorov length and time scales, respectively. Each line represents a different initial separation, $l_0/\eta = \frac{1}{4}$, 1, 4, 16, 32, and 64 for lines A–F, respectively. The solid lines are Yeung's (Ref. 1) DNS results and the dashed lines are the present KS results for energy spectrum 4 in Fig. 1. Lines of slope equal to $\frac{1}{2}$ and 1 are shown for comparison. The KS input energy spectrum is case 4 of Fig. 1 with $N_{kI} = 50$ modes in the inertial part of the spectrum.

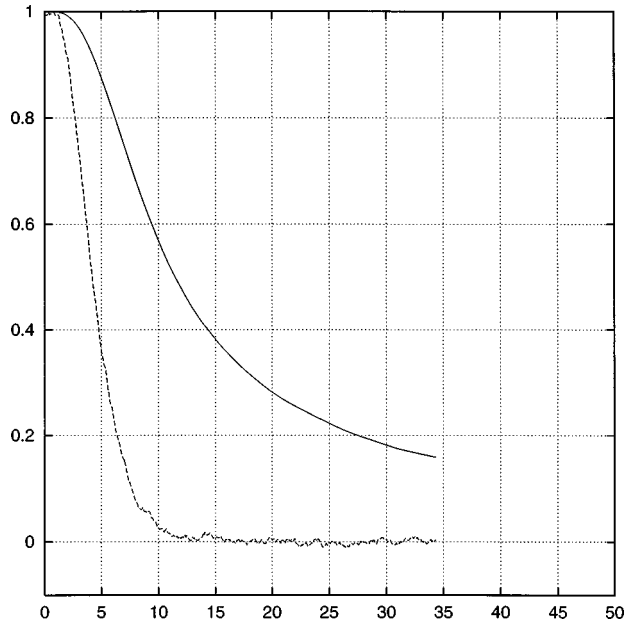

FIG. 3. Evolution of the correlation coefficients between particle pair displacements, $\rho(y_i^{(1)}, y_i^{(2)})$ (solid line), and velocity components $\rho(u_i^{(1)}, u_i^{(2)})$ (dashed line), against t/T_L for case A, $l_0 = \frac{1}{4}$, from KS. T_L is the Lagrangian time scale. The KS input energy spectrum is case 4 of Fig. 1.

statistics are drawn from as many flow field realizations as particle pairs. The agreement with Yeung's DNS results is good; this agreement is only marginally worse when $\lambda = 0$, but it is significantly worse for the small values of t/τ_η if the high-wave number viscous range of $E(k)$ is not taken into account (as for cases 1 and 2). We also find that the inclusion or exclusion of the low-wave number end of the spectrum (the difference between cases 3 and 4) makes no appreciable difference to the KS results of Fig. 2, except obviously for long times, $t/T_L \gg 1$, when the separation of particles is larger than the integral length scale L and the inclusion or exclusion of energy in the largest scales will affect the long time regime that asymptotes to the Taylor diffusion law $\sim (2u'^2 T_\mathrm{L})t$.

Yeung also defines the displacement $\mathbf{y(t)} = \mathbf{x(t)} - \mathbf{x(0)}$ for a particle and calculates the correlation coefficients $\rho(y_i^{(1)}, y_i^{(2)})$ and $\rho(u_i^{(1)}, u_i^{(2)})$ as functions of time t/T_L. In Fig. 3 we plot the results for $\rho(y_i^{(1)}, y_i^{(2)})$ and $\rho(u_i^{(1)}, u_i^{(2)})$ versus time from KS. The comparison with Yeung's corresponding Fig. 3 is good. Keeping to Yeung's order of results, in Fig. 4 we plot $\rho(u_i^{(1)}, u_i^{(2)})$ versus time for the same six initial separations as above. The comparison between the DNS and the KS results is good, again, and better for $\lambda = 0.4$ than for $\lambda = 0$. An increased value of λ implies an increased decorrelation, and therefore the KS correlation coefficients $\rho(y_i^{(1)}, y_i^{(2)})$ and $\rho(u_i^{(1)}, u_i^{(2)})$ are smaller for larger values of λ. The statistics of Figs. 3 and 4 are the only ones among those calculated by Yeung that are significantly sensitive to the unsteadiness parameter λ. $\rho(u_i^{(1)}, u_i^{(2)})$ are, however, not sensitive to the differences between energy spectra inputs 1–4 (Fig. 1), except for the largest initial separation $l_0/\eta = 64$; which is so large that it is already of the order of an integral length scale L. $\rho(y_i^{(1)}, y_i^{(2)})$ in Fig. 3 decorrelates a little faster in case 1 because of the exclusion of the largest scales.

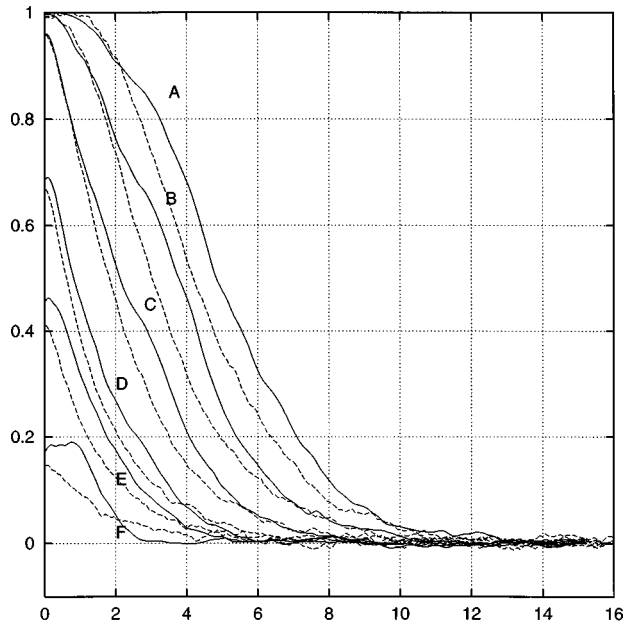

FIG. 4. Evolution of the correlation coefficients between particle pair velocities, $\rho(u_i^{(1)}, u_i^{(2)})$ against t/T_L, for initial separations $l_0/\eta = \frac{1}{4}$, 1, 4, 16, 32, and 64 for lines A–F. Solid lines are Yeung's (Ref. 1) DNS results, and the dashed lines are the KS results. Each set of results are normalized by their respective Lagrangian length scales, T_L. The KS input energy spectrum is case 4 of Fig. 1.

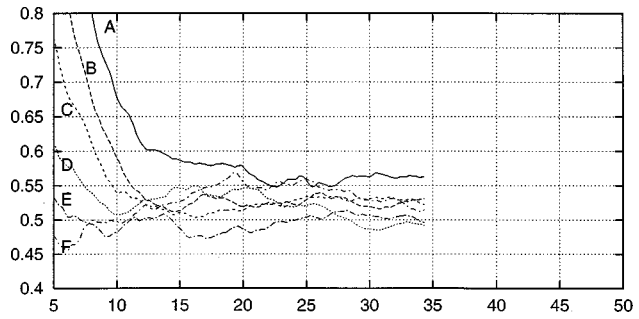

FIG. 5. Evolution of the skewness coefficient (μ_3) of the separation distance l against t/T_L for the same initial separations as in Fig. 4 for lines A–F [cf. Yeung's (Ref. 1). Fig. 8(a)]. The KS input energy spectrum is case 4 of Fig. 1.

Yeung's Fig. 5 is effectively a replot of his Fig. 4. Again, the KS predictions for $\lambda = 0.4$ are in good agreement with Yeung's Fig. 5, but we do not present them here for economy of space. Also, for economy of space we do not present the KS equivalents of Yeung's Figs. 6 and 7, which demonstrate that for times significantly longer that the integral time scale T_L, the PDF of l_i is Gaussian and that of $|\mathbf{l}|^2$ is chi square. As expected, these conclusions hold in KS as they do in DNS, and, in fact, as they would do in any random process with a finite value of T_L.

Yeung's Figs. 8 and, especially 9, deserve more attention. Yeung plots the skewness coefficients and flatness factors of the separation distance $l(t) = |\mathbf{l}(\mathbf{t})|$ as functions of t/T_L in his Figs. 8(a) and 8(b), and the flatness factors $\mu_4(t, l_0)$ of one component of the relative velocity $\mathbf{w}(t) = \mathbf{u}^{(1)}(t) - \mathbf{u}^{(2)}(t)$ as a function of t/τ_η in his Fig. 9. The results of KS calculations of skewness coefficients and flatness factors of l for different initial separation distances l_0 (see Figs. 5 and 6) do not depend significantly on the unsteadiness parameter λ (in the range $0 < \lambda < 1$), but they are quite sensitive to the low-wave number end of the input energy spectrum. Figures 5 and 6 have been obtained for energy spectrum case 4 (Fig. 1) and compare well with Yeung's equivalent Figs. 8(a) and 8(b). While similar results from KS are obtained for case 2, the exclusion of the low-wave number part of the spectrum in cases 1 and 3 leads to overestimated values of the skewness coefficients and flatness factors of l, even at the larger values of t/T_L shown in these figures.

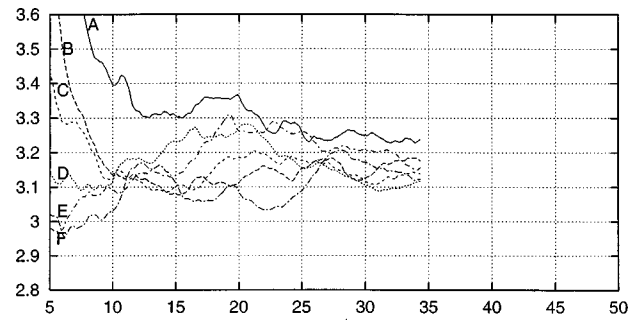

FIG. 6. Evolution of the flatness factor (μ_4) of the separation distance l against t/T_L for the same initial separations as in Fig. 4 for lines A–F [cf. Yeung's (Ref. 1). Fig. 8(b)]. The KS input energy spectrum is case 4 of Fig. 1.

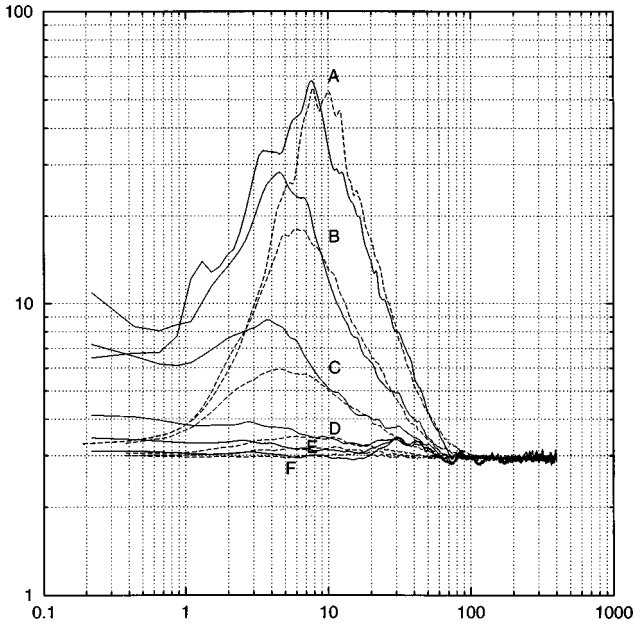

FIG. 7. Evolution of the flatness factor μ_4 of the relative velocity (component) w_1 vs t/τ_η, for initial separations $l_0/\eta = \frac{1}{4}$, 1, 4, 16, 32, and 64 for lines A–F. The solid lines are Yeung's (Ref. 1) DNS results and the dashed lines are the KS results. The Gaussian value is 3. τ_η is the Kolmogorov time scale. The KS input energy spectrum is case 4 of Fig. 1.

Yeung's results for the flatness factor of the relative velocity $\mu_4(t, l_0)$, his Fig. 9, is important not only because this quantity defines a concept of Lagrangian intermittency (see Sec. IV) but also because KS is able to match the DNS results remarkably well, whereas Heppe's[2] stochastic model of two-particle dispersion is some way off. The DNS and KS results for $\mu_4(t)$ are plotted in Fig. 7 for the same initial separations l_0/η as before; the peak values of the respective plots differ by no more than a factor of 1.3 for the best case (A: $l_0/\eta = \frac{1}{4}$) and 1.8 for the worst case (B: $l_0/\eta = 1$). Moreover, the peaks in the KS plots occur at about the same times as in the DNS results; see Table II. Heppe's[5] stochastic model of two-particle dispersion does not reproduce these DNS results to the same degree of accuracy, even with the most favorably adjusted input parameters, but leads to peak values in $\mu_4(t, l_0)$, which underestimate the DNS peak values by factors ranging between 5 and 8. The KS results for $\mu_4(t)$ are only marginally better for $\lambda = 0.4$ than $\lambda = 0$, and they do not depend on the very high- and very low-wave

TABLE II. A comparison of DNS [Yeung (Ref. 1)] and KS (case 4) results, $Re_\lambda = 91$.

	DNS				KS			
l_0/η	μ_4^{peak}	T_L/τ_η	t_{peak}/τ_η	T_L/t_{peak}	μ_4^{peak}	T_L/τ_η	t_{peak}/τ_η	T_L/t_{peak}
0.25	80	8.7	8	1.1	60	8	8	1
1	28	8.7	4.5	1.9	16	8	6	1.3
4	8.8	8.7	4	2.2	5.8	8	4	2

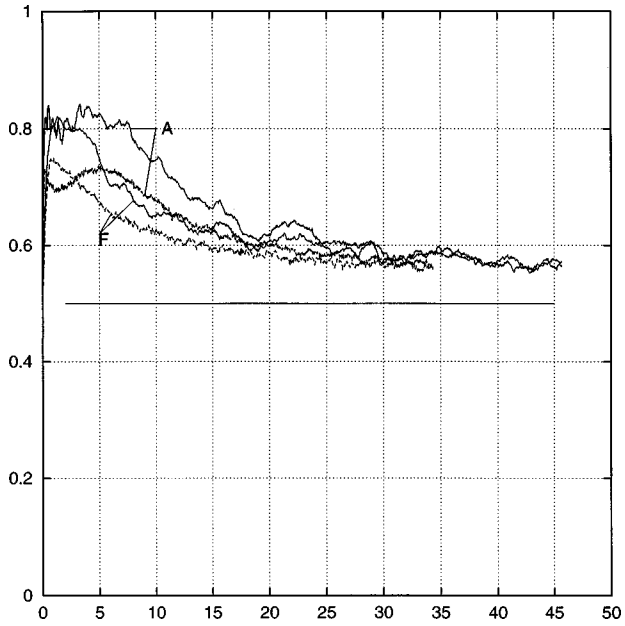

FIG. 8. Evolution of the probability of acute alignment between the separation and relative velocity vectors, $P[0<\theta<90°]$, against t/T_L for initial separations $l_0/\eta=\frac{1}{4}$ (A) and 64 (F). Solid lines are Yeung's (Ref. 1) DNS results and dashed lines are the KS results. The KS input energy spectrum is case 4 of Fig. 1.

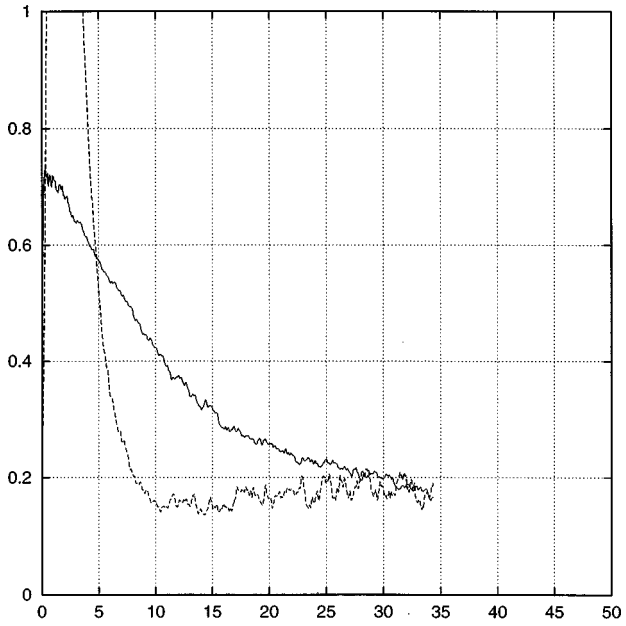

FIG. 9. Evolution of the correlation coefficient $\rho(l,w)$ (solid line) between l and w_l, and the modified correlation function $\rho^*(l,w_l)$ (dashed line), against t/T_L for initial separation $l_0/\eta=\frac{1}{4}$ [cf. Yeung's (Ref. 1) Fig. 14(a)]. The KS input energy spectrum is case 4 of Fig. 1.

number ends of the energy spectrum (the results are similar for all cases 1–4) for large Reynolds number, as we show in Sec. IV.

This dramatic quantitative difference between the flatness factor predictions of stochastic models and KS may be a reflection of the qualitative difference between the two underlaying mechanisms for two-particle dispersion in the respective models. In two-particle stochastic models, Lagrangian relative velocities are solutions of Langevin-type equations and depend on Wiener processes, which means that particle pairs separate gradually by a constantly operating decorrelation mechanism. However, in KS particle pairs do not separate gradually but in bursts, when they meet straining regions (Malik,[12] Fung *et al.*,[2] Fung and Vassilicos[3]), and spend most of the time before such rare and violent events traveling close together. Hence, the absolute value of the relative velocity $\mathbf{w}(t)=\mathbf{u}^{(1)}(t)-\mathbf{u}^{(2)}(t)$ may be expected to be more often either close to 0 or very large in KS than in stochastic models, thus leading to significantly higher values of $\mu_4(t,l_0)$ in KS than in Heppe's[5] stochastic model. Indeed, the KS prediction for $\mu_4(t)$ is in good agreement with Yeung's DNS, whereas Heppe's[5] stochastic model prediction for $\mu_4(t)$ significantly underestimates the peak values.

Two sets of results of Yeung's DNS remain that merit attention in this paper. Yeung defines the angle θ between the separation vector $\mathbf{l}(t)$ and the relative velocity vector $\mathbf{w}(t)$ and computes the probability $P(0<\theta<\pi/2)$ of acute alignment between $\mathbf{l}(t)$ and $\mathbf{w}(t)$ (which is equivalent to the probability that the two particles are moving apart) as a function of time t/T_L. We plot $P(0<\theta<\pi/2)$ against t/T_L in Fig. 8. The KS prediction for $P(0<\theta<\pi/2)$ does not differ significantly with λ or with the energy input; the agreement between KS and DNS in all cases is satisfactory.

Finally, we plot in Figs. 9 and 10 correlation coefficients $\rho(l,w_l)$ between the separation distance l and $w_l=(d/dt)l=|\mathbf{w}|\cos\theta$, as well as ''modified correlation coefficients'' $\rho^*=\langle l w_l\rangle/\langle l\rangle\langle w_l\rangle-1$, both as functions of t/T_L. Again, the agreement with Yeung's equivalent Fig. 14 is satisfactory and is similar for $\lambda=0$ and for all energy spectrum cases 1–4.

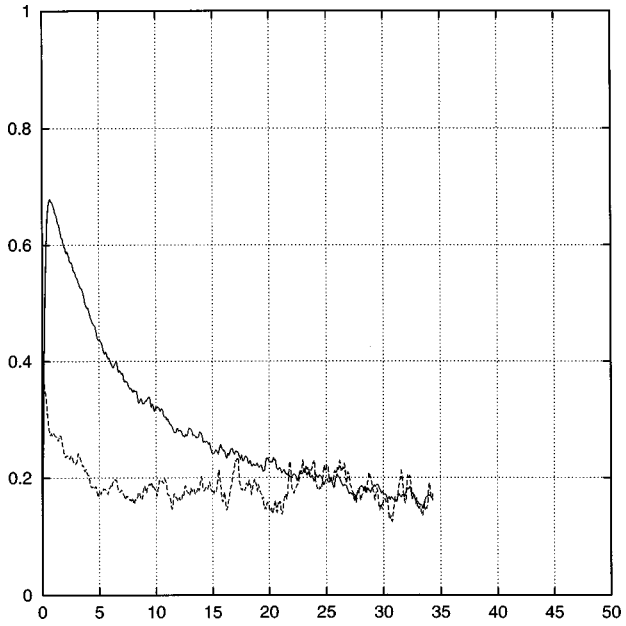

FIG. 10. Evolution of the correlation coefficient $\rho(l,w)$ (solid line) between l and w_l, and the modified correlation function $\rho^*(l,w_l)$ (dashed line), against t/T_L for initial separation $l_0/\eta=64$ [cf. Yeung's (Ref. 1) Fig. 14(b)]. The KS input energy spectrum is case 4 of Fig. 1.

IV. THE FLATNESS FACTOR AS A FUNCTION OF REYNOLDS NUMBER

Let us now concentrate attention on the flatness $\mu_4(t)$ because of its relation to intermittency. In the Eulerian frame, a quantitative definition of intermittency is usually given in terms of the flatness $F(r)=\langle[u_E(x+r)-u_E(x)]^4\rangle/\langle[u_E(x+r)-u_E(x)]^2\rangle^2$, where $u_E(x)$ is an Eulerian velocity component. If a field is Gaussian, and therefore not intermittent, $F(r)=3$ for all r. The Eulerian velocity field is said to be intermittent when $F(r)$ increases with decreasing r (see Frisch[13]). Similarly, we may refer to Lagrangian intermittency when $\mu_4(t)$ increases with decreasing t.

Eulerian laboratory measurements of $F(r)$ show that $F(r)$ increases above the Gaussian value of 3 with decreasing r in the inertial range and reaches a maximum value at a small value of r that is related to the dissipation range (Tabeling *et al.*[14]). No Lagrangian laboratory measurements of $\mu_4(t)$ are currently available, and DNS measurements of $\mu_4(t)$ are limited to relatively small Reynolds numbers. At $\mathrm{Re}_\lambda \approx 91$, Yeung's DNS and the present KS show that $\mu_4=3$ for times t larger than approximately eight Lagrangian integral time scales, T_L, and increases quite dramatically with decreasing t below $8T_L$ if the initial distance l_0 between the two fluid elements is of order η (Fig. 7). For $l_0=\frac{1}{4}\eta$, the flatness μ_4 reaches a peak value of approximately 80 (DNS) and 60 (KS) at a time $t_{peak}/\tau_\eta \approx 8$ for both the DNS and the KS. As t/τ_η decreases below t_{peak}/τ_η, μ_4 decreases for all these values of l_0/η; the results for $l_0/\eta=\frac{1}{4}$, 1, and 4 are summarized in Table II. The Reynolds number in these simulations is low, and so there is not enough separation between large and small scales to see whether t_{peak} is of order τ_η or of order T_L.

The behavior of μ_4 and the scaling of t_{peak} with increasing Reynolds number cannot be tested with DNS at present, and it remains unknown how $\mu_4(t)$ behaves in the inertial time range, $\tau_\eta \ll t \ll T_L$, at high Reynolds numbers, and whether t_{peak} scales with the viscous time scale τ_η, or with the Lagrangian time scale T_L or perhaps even some other time scale (perhaps the Taylor microscale, which is intermediate between τ_η and T_L?). Heppe's[5] stochastic model of two-particle dispersion that has been adjusted to incorporate Reynolds number effects predicts that $t_{peak}=O(\tau_\eta)$ and $\mu_4=3$ for $t \gg \tau_\eta$ for *all Reynolds numbers*.

In view of the good quantitative agreement in Lagrangian statistics between DNS and KS for $\mathrm{Re}_\lambda \approx 91$, it may be interesting to use KS to predict $\mu_4(t)$ for large Reynolds numbers, which can be easily generated in KS models by increasing k_η/k_0 at a relatively moderate expense. What does the KS model of two-particle dispersion, which incorporates small-scale turbulent-like flow structures, predict for the behavior of $\mu_4(t)$ in the inertial time range and for the scaling of t_{peak} for large Reynolds numbers?

In Fig. 11 we plot the flatness factor $\mu_4(t)$ for $k_I/k_L=5$, 100, and 400 for the case A when $l_0/\eta=\frac{1}{4}$. We define a corresponding Reynolds number $\mathrm{Re}\equiv(k_I/k_L)^{4/3}=8.5$, 464, and 2947 for these simulations. The energy spectrum in these new simulations is similar to case 4 of Fig. 1, but with $N_{kI}=150$ modes for $k_I/k_L=100$ and $N_{kI}=250$ for $k_I/k_L=400$ see Table I. We have kept the same value for α_K so that we are adding small amounts of energy to the flow by simply extending the inertial range part of spectra to higher-wave numbers k_I, which then falls off exponentially for $k>k_I$. The Lagrangian integral time scale T_L remains the same because this quantity is determined by the large scales. But the Kolmogorov time microscale decreases with k_η because $\tau_k \sim k_\eta^{-2/3}$. The key new feature that emerges is that the Lagrangian flatness factor is significantly greater than 3 *over a wide range of inertial time scales*, $\tau_\eta < t < 8T_L$, for these Reynolds numbers. Note that $\mathrm{Re}=8.5$ corresponds to Yeung's $\mathrm{Re}_\lambda=91$. Making use of the relation $\mathrm{Re}_\lambda \propto \mathrm{Re}^{1/2}$, we find that $\mathrm{Re}_\lambda \approx 670$ for $\mathrm{Re}=464$, and $\mathrm{Re}_\lambda \approx 1690$ for $\mathrm{Re}=2947$. Furthermore, the peak value in the flatness μ_4 increases from 60 to about 100 and 200, respectively, while the nondimensional time t_{peak}/τ_η at which the peak occurs appears to increase only very slowly; respectively, about 8, 10, and 13, and these correspond to $T_L/t_{peak} \approx 1$, 6, and 12, respectively. These results are summarized in Table III. Certainly, we cannot conclude that t_{peak} scales with either T_L or

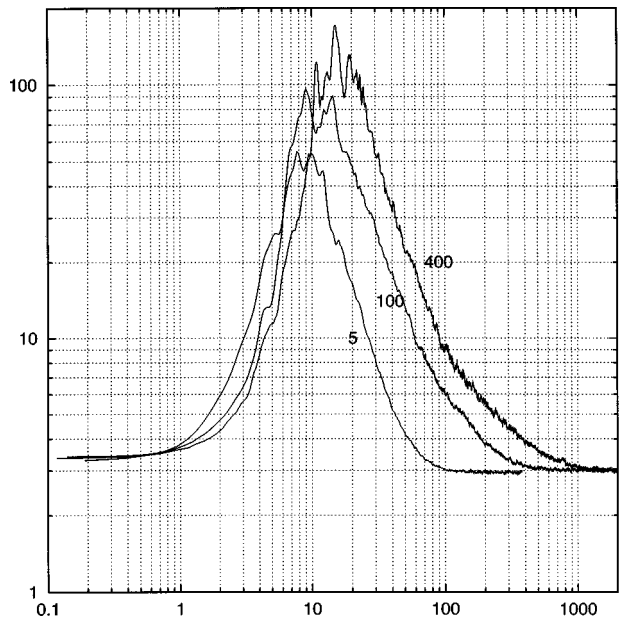

FIG. 11. Evolution of the flatness factor μ_4 of the relative velocity (component) w_1 vs t/τ_η from KS with different inertial ranges, $k_I/k_L=5$ (from Fig. 7), 100, and 400. The initial separation in each case is $l_0/\eta=\frac{1}{4}$ (A). The time is normalized by the respective Kolmogorov time scale in each case. The KS input energy spectrum is case 4 of Fig. 1 with $N_{kL}=50$, $N_{kI}=50$, and $N_{kH}=5$ modes for $k_I/k_L=5$, $N_{kL}=50$, $N_{kI}=150$, and $N_{kH}=5$ for $k_I/k_L=100$ and $N_{kL}=50$, $N_{kI}=250$, and $N_{kH}=5$ modes for $k_I/k_L=400$. See Table I.

TABLE III. DNS [Yeung (Ref. 1)] and KS (case 4) results for different Reynolds numbers ($l_0/\eta=0.25$).

Case	k_I/k_L	k_η/k_L	Re	Re_λ	μ_4^{peak}	t_{peak}/τ_η	T_L/t_{peak}
DNS	5	25	8.5	91	80	8	1.1
4	5	25	8.5	91	60	8	1
4	100	500	464	670	100	10	6
4	400	2000	2947	1690	200	13	12

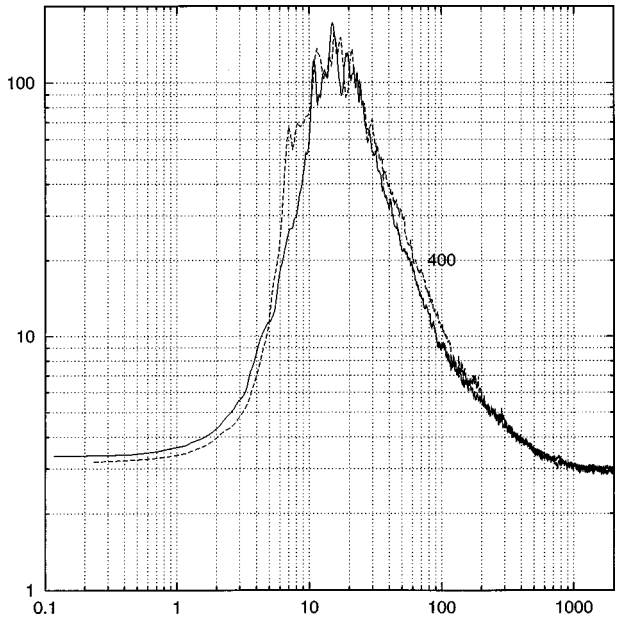

FIG. 12. A comparison of the evolution of the flatness factor μ_4 of the relative velocity (component) w_1 vs t/τ_η between cases 2 and 4 of Fig. 1 for $k_I/k_L=400$. All details are the same as those in Fig. 11, except that for case 2 (dashed line) $N_{kH}=0$. See Table I.

τ_η. We can only conclude from these simulations that the values of the flatness factor are significantly larger than 3 over a substantial range of times bounded from below by τ_η and above by $8T_L$.

Finally, a question of considerable interest is how sensitive is the behavior of the flatness factor $\mu_4(t)$ to the nature of the transition between the dissipation subrange and the inertial range, particularly for high Reynolds numbers. To test this in the KS model, we have performed some simulations with case 2 of Fig. 1 as the input spectrum. In case 2, $E(k)=0$ for $k_I<k\leqslant k_\eta$, in contrast to Yeung's spectrum case 4. We confirm that the results for the behavior of $\mu_4(t)$ in the inertial time range obtained from case 2 is similar to those obtained from case 4 in Fig. 11. For example, Fig. 12 shows the comparison in $\mu_4(t)$ for $k_I/k_L=400$ ($k_\eta/k_L=2000$) between cases 2 and 4 (all other input parameters being identical); there is no significant difference between the two cases in the inertial time range.

V. CONCLUSION

In this paper we have compared the results on two-particle relative statistics from Yeung's[1] DNS for statistically isotropic and stationary turbulence with the corresponding results from KS. The comparison between DNS and KS results for the same parameter values was good in most of the statistics and satisfactory in a few. This, to our knowledge, is the first direct comparison between DNS and KS and, as such, constitutes the first validation test for KS as a serious *Lagrangian* modeling tool for fluid particle dispersion in homogeneous, isotropic turbulence. We believe the results contained in this paper justify this claim. We emphasize here, again, that the *physical* input to the KS model is just the Eulerian wave number spectrum $E(k)$ and the dimensionless constant λ that is a temporal decorrelation parameter. On physical grounds $\lambda=O(1)$, and we have taken $\lambda=0.4$. In fact, we have shown that most of the statistics are not significantly affected even when $\lambda=0$, so that this parameter could be effectively removed as an input leaving just $E(k)$ alone to define the entire structured flow and the induced dispersion processes that ensues from it. This is a remarkable reduction in input complexity. Furthermore, let us note that whereas DNS takes $O(10^6)$ degrees of freedom to produce the Lagrangian statistics, KS takes $O(10^2)$ to generate quantitatively similar results.

Of particular interest is the flatness factor of the two-particle relative velocity components, $\mu_4(t,l_0)$, which is a measure of Lagrangian intermittency. The KS predicts Yeung's DNS result for $\mu_4(t)$ remarkably well (Fig. 7). This lends support to the idea that two-particle turbulent dispersion is well modeled as bursts in separation, when particle pairs meet straining flow regions (Malik,[12] Fung *et al.*,[2] and Fung and Vassilicos[3]). Some experimental evidence supporting this picture is contained in Virant and Dracos,[9] where in Fig. 8(d) a pair of particle trajectories show a process of separation similar to that just described. Such a process is readily obtained in the KS model, which contains genuine turbulent-like flow structures (eddying, straining, and streaming structures), which yield qualitatively realistic particle trajectories. Our results indicate that the Lagrangian statistics of these KS trajectories are quantitatively realistic as well.

The KS model was then used to look at the behavior of the flatness factor $\mu_4(l_0,t)$ for large Reynolds numbers $\mathrm{Re}=(k_I/k_L)^{4/3}=464$ and 2947, which correspond to $\mathrm{Re}_\lambda\approx 670$ and 1690, respectively. Our results for the flatness factor $\mu_4(t)$ (Fig. 11) shows that μ_4 is significantly greater than the Gaussian value of 3 over a substantial part of the inertial time range.

ACKNOWLEDGMENTS

We gratefully acknowledge financial support from the Royal Society, the E.P.S.R.C., the Hong Kong Research Grant Council, the European Union under a Marie-Curie Fellowship, an Alliance 1996 project run jointly by the French Ministry of Foreign Affairs and the British Council. The authors are grateful to Professor P. K. Yeung for making available his DNS data. Computational resources were made available on the Cambridge High Performance Computing Facility.

[1] P. K. Yeung, ''Direct numerical simulation of two-particle relative diffusion in isotropic turbulence,'' Phys. Fluids **6**, 3416 (1994).
[2] J. C. H. Fung, J. C. R. Hunt, N. A. Malik, and R. J. Perkins, ''Kinematic simulations in turbulent flow generated by unsteady random Fourier modes,'' J. Fluid Mech. **236**, 281 (1992).
[3] J. C. H. Fung and J. C. Vassilicos, ''Two-particle dispersion in turbulent-like flow,'' Phys. Rev. E **57**, 1677 (1998).
[4] M. S. Chong, J. Soria, A. E. Perry, J. Chacin, B. J. Cantwell, and Y. Na, ''Turbulence structures of wall-bounded shear flows found using DNS data,'' J. Fluid Mech. **357**, 225 (1998).
[5] B. M. O. Heppe, ''Generalised Langevin equations for relative turbulent dispersion,'' J. Fluid Mech. **357**, 167 (1998).
[6] G. Pedrizzetti and E. A. Novikov, ''On Markov modelling of turbulence,'' J. Fluid Mech. **280**, 69 (1994).

[7]M. S. Borgas and B. L. Sawford, ''A family of stochastic models for two-particle dispersion in isotropic homogeneous stationary turbulence,'' J. Fluid Mech. **279**, 69 (1994).
[8]N. A. Malik, ''Structural diffusion in 2D and 3D random flows,'' in *Advances In Turbulence VI*, edited by S. Gavrilakis *et al.* (Kluwer Academic, Netherlands, 1996), pp. 619–620.
[9]M. Virant and Th. Dracos, ''3D PTV and its application on Lagrangian motion,'' Meas. Sci. Technol. **8**, 1539 (1997).
[10]H-G. Maas, A. W. Gruen, and D. A. Papantoniou, ''Particle tracking velocimetry in three dimensional flows. Part I: The imaging technique,'' Exp. Fluids **15**, 133 (1993).
[11]N. A. Malik, Th. Dracos, and D. A. Papantoniou, ''Particle tracking velocimetry in three dimensional flows. Part II: Particle tracking,'' Exp. Fluids **15**, 279 (1993).
[12]N. A. Malik, ''Studies in turbulent dispersion using Kinematic Simulation,'' Ph.D. thesis, Cambridge, 1991.
[13]U. Frisch, *Turbulence: The Legacy of A. N. Kolmogorov* (Cambridge University Press, Cambridge, 1995).
[14]P. Tabeling, G. Zocchi, F. Belin, J. Maurer, and H. Willaime, ''Probability density functions, skewness and flatness in large Reynolds number turbulence,'' Phys. Rev. E **53**, 1613 (1996).